TREM2 haplodeficiency in mice and humans impairs the microglia barrier function leading to decreased amyloid compaction and severe axonal dystrophy

Supplemental Information

Peng Yuan[1,2*], Carlo Condello[1*#], C. Dirk Keene[3], Yaming Wang[4], Thomas D. Bird[5], Steven M. Paul[6], Wenjie Luo[6], Marco Colonna[4], David Baddeley[7,8], Jaime Grutzendler[1,2§]

1) Department of Neurology, Yale University, New Haven, CT 06510, USA
2) Department of Neuroscience, Yale University, New Haven, CT 06511, USA
3) Department of Pathology, University of Washington, Seattle, WA98195, USA
4) Department of Pathology and Immunology, Washington University School of Medicine, St. Louis, MO 63110, USA
5) Department of Neurology, University of Washington, Seattle, WA98195, USA
6) The Helen and Robert Appel Alzheimer's Disease Research Institute, Brain and Mind Research Institute, Weill Cornell Medical College, New York, NY10065, USA
7) Department of Cell Biology, Yale University, New Haven, CT 06511, USA
8) Nanobiology Institute, Yale University, West Haven, CT 06515, USA

*These authors contributed equally

#Present address: Department of Neurology, University of California San Francisco, 94158 USA

§Corresponding author: 300 George Street, 8300G, New Haven, CT 06511, jaime.grutzendler@yale.edu

Figure S1 (related to Figure 1)

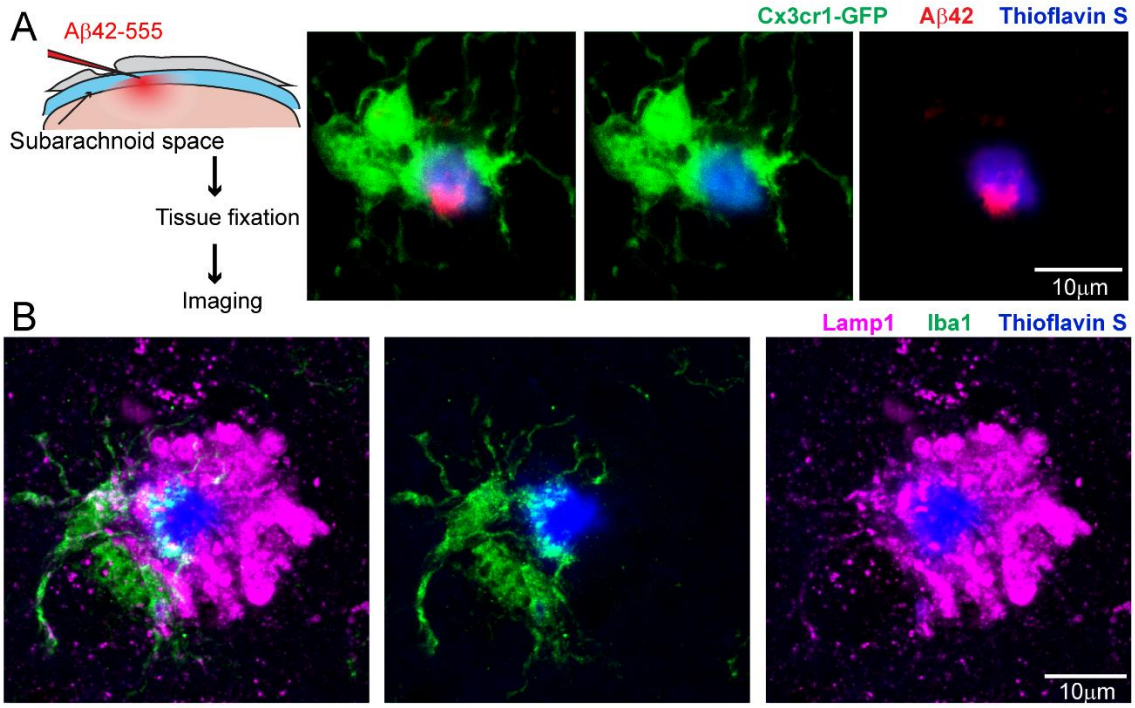

Microglia processes form a barrier that prevents toxic accumulation of Aβ42 hotspots leading to reduced neuritic dystrophy in microglia-covered areas.

(**A**) Soluble Aβ42 (red) preferentially incorporates into existing plaques (blue) at hotspot microregions lacking microglia barrier (green). Fluorescently labeled Aβ42 was infused into the subarachnoid space as described and tissue was fixed for imaging. Areas not covered by microglia have greater Aβ42 binding because the density of amyloid fibrils is lower (Condello et. al. 2015). The precise reason for the greater affinity to these uncovered areas is not clear. (**B**) Areas covered by microglia processes (green) are associated with less axonal dystrophy (labeled by a Lamp1 antibody; magenta) around plaques (blue). Neuronal processes near areas not covered by microglia processes are exposed to higher concentrations of toxic protofibrillar Aβ42 which leads to greater neuritic injury (Condello et. al. 2015).

Figure S2 (related to Figure 1)

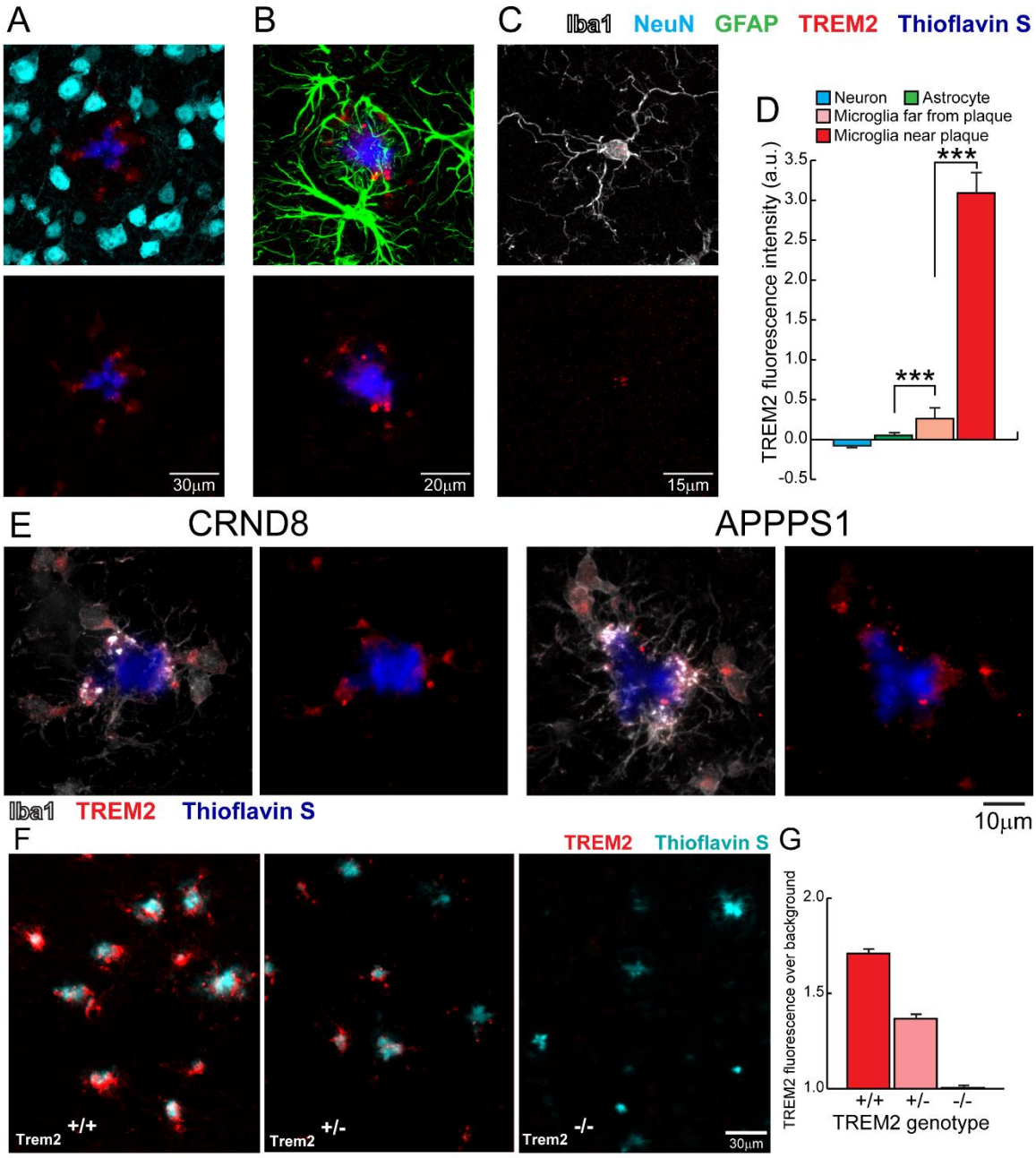

Trem2 is preferentially upregulated in plaque-associated microglia

Confocal images showing lack of Trem2 immunoreactivity within NeuN-labeled neurons (**A**) and GFAP-labeled astrocytes (**B**). Iba1-labeled microglia (white) far from plaques (**C**) have minimal Trem2 expression in the cell soma. (**D**) Quantification of fluorescence intensity of Trem2 in different cell types. N=3 animals, 150 neurons, 117 astrocytes and 150 microglia were analyzed. (**E**) Additional examples of Trem2 staining in CRND8 and APPPS1 transgenic AD mouse models. (**F**) Example images of Trem2 immunostaining in 5XFAD mice with Trem2 +/+, Trem2 +/- and Trem2 -/- genotype. (**G**) Quantification of Trem2 fluorescence intensity in brains of 5XFAD mice with different copy numbers of the Trem2 gene. N=3 mice for each group. Student t-tests were used for statistical comparisons, ***: $p<0.001$.

Figure S3 (related to Figure 2 and Figure 4)

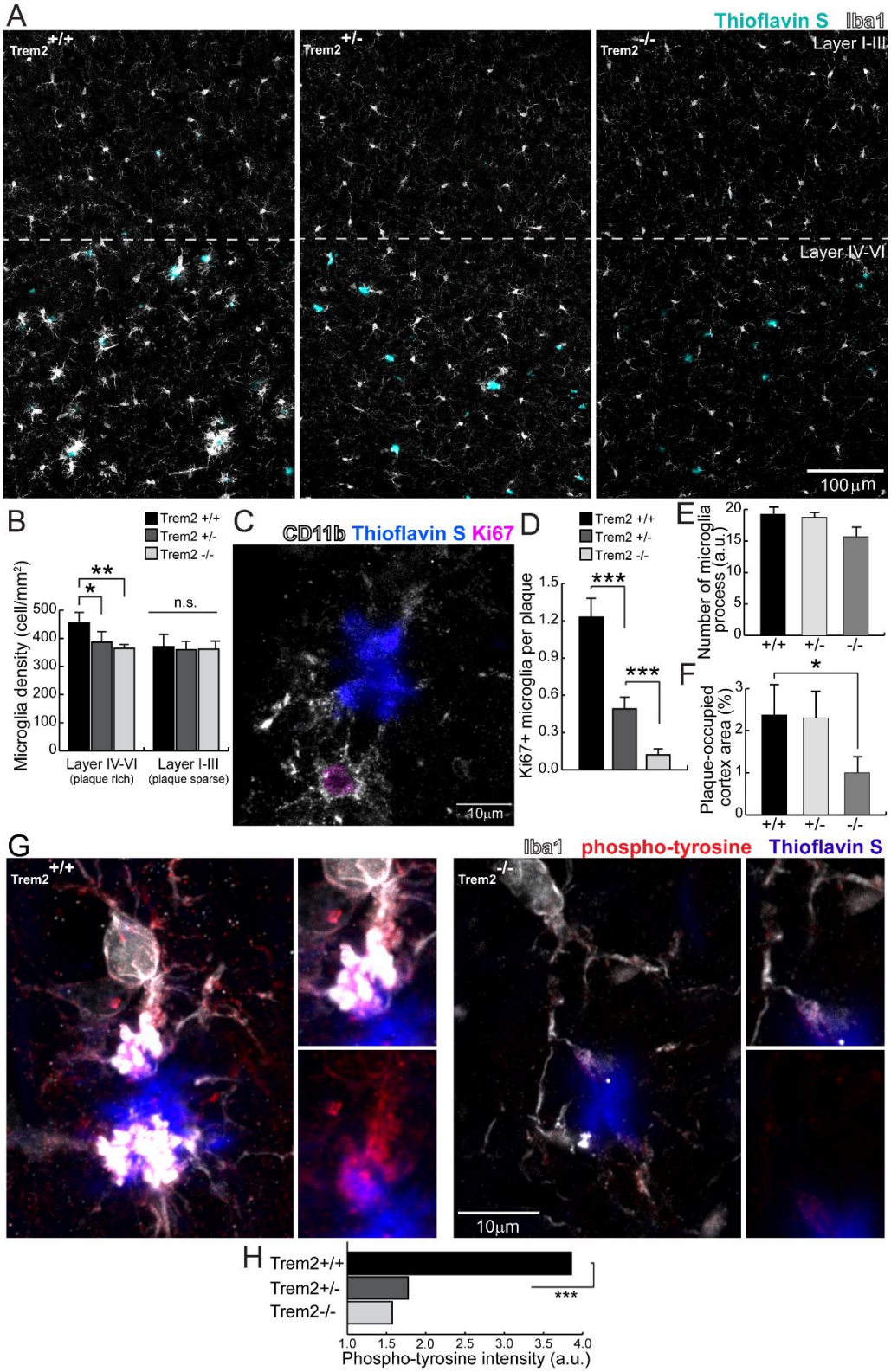

Trem2 deficiency diminishes the proliferative capacity of microglia in plaque-rich regions

(**A**) Confocal images of Iba1-immunolabeled microglia (white) thioflavin-positive amyloid plaques (cyan) in 5XFAD mice with different copy numbers of the Trem2 gene. (**B**) Cell number quantification of microglia in plaque-rich cortical layers IV-VI compared to plaque-free cortical layers I-III. N=3 mice for each group, total 1993 microglia analyzed. (**C**) Confocal images of proliferation marker Ki67-immunohistochemistry (magenta) within Iba1-immunopostive microglia (white) around thioflavin s-positive amyloid plaques (blue). (**D**) Quantification of Ki67-positive proliferating microglia per plaque in 5xFAD mice with different Trem2 genotypes. (**E**) Quantification of the amount of microglia processes around individual cell soma as measured by thresholded area of Iba1-immunolabeled processes. N=3 mice for each group, total 540 microglia were analyzed. See also **Figure 2**. (**F**) Quantification of total cortical area occupied by 4G8 positive amyloid plaques in 5XFAD mice with different copy numbers of Trem2 gene. Two brain slices were analyzed for each mouse and N=3 mice for each group. See also **Figure 4**. (**G**) Confocal images of phospho-tyrosine immunoreactivity (red) in plaque-associated Iba1-positive microglia (white) around thioflavin S-positive amyloid plaques (blue) microglia in Trem2 +/+ (left panels) and Trem2 -/- (right panels) 5xFAD brain slices. (**H**) Quantification of phospho-tyrosine levels in plaque-associated microglia in 5xFAD mice with different Trem2 genotypes. N=3 mice for each group, 450 cells were analyzed. Student t-tests were used for statistical comparisons, *: $p<0.05$, **: $p<0.01$, ***: $p<0.001$; a.u.: arbitrary unit. All analyses were performed with neocortical plaques.

Figure S4 (related to Figure 2)

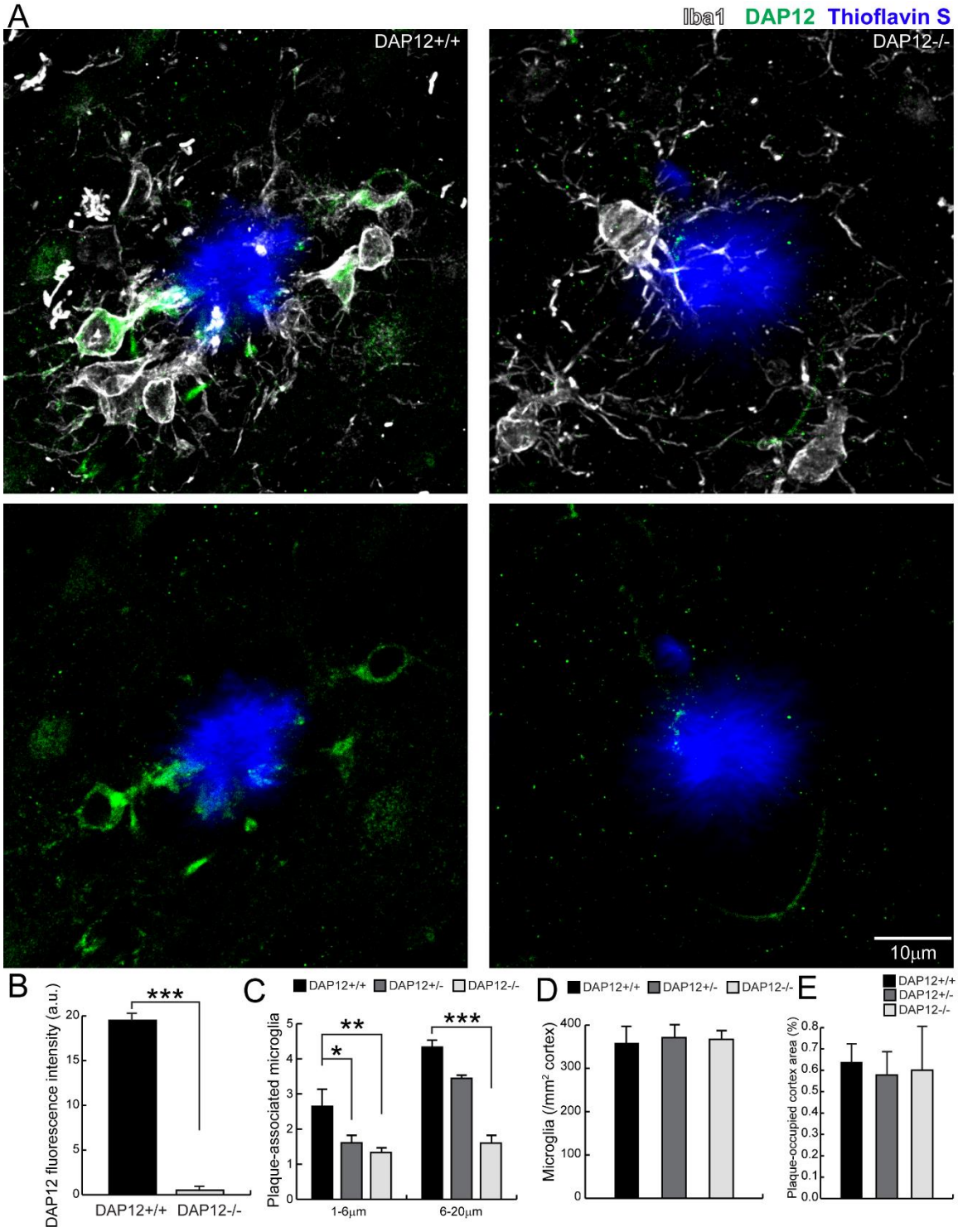

DAP12 deficiency abolishes microglia recruitment around amyloid plaques

(**A**) Confocal images of DAP12 staining within the Iba1-immunolabeled microglia (white) around thioflavin-positive amyloid plaques (blue) in APPPS1 mice with and without DAP12 gene. (**B**) Quantification of DAP12 fluorescence around amyloid plaques in DAP12 +/+ and -/- mice. 30 plaques were analyzed for each group. (**C-D**) Quantification of the number of microglia cells associated and far away from amyloid plaques. Total 163 plaques were analyzed. For all quantifications N=3 animals for each group. Student t-tests were used for statistical comparisons, *: $p<0.05$, **: $p<0.01$, ***: $p<0.001$; a.u.: arbitrary unit. All analyses were performed with neocortical plaques. (**E**) Quantification of the total percentage cortical area occupied by amyloid plaque in APPPS1 mice with and without DAP12 gene. Amyloid plaques were stained with 4G8 immunohistochemistry. Two brain slices were analyzed for each mouse and N=3 animals for each group.

Figure S5 (related to Figure 3)

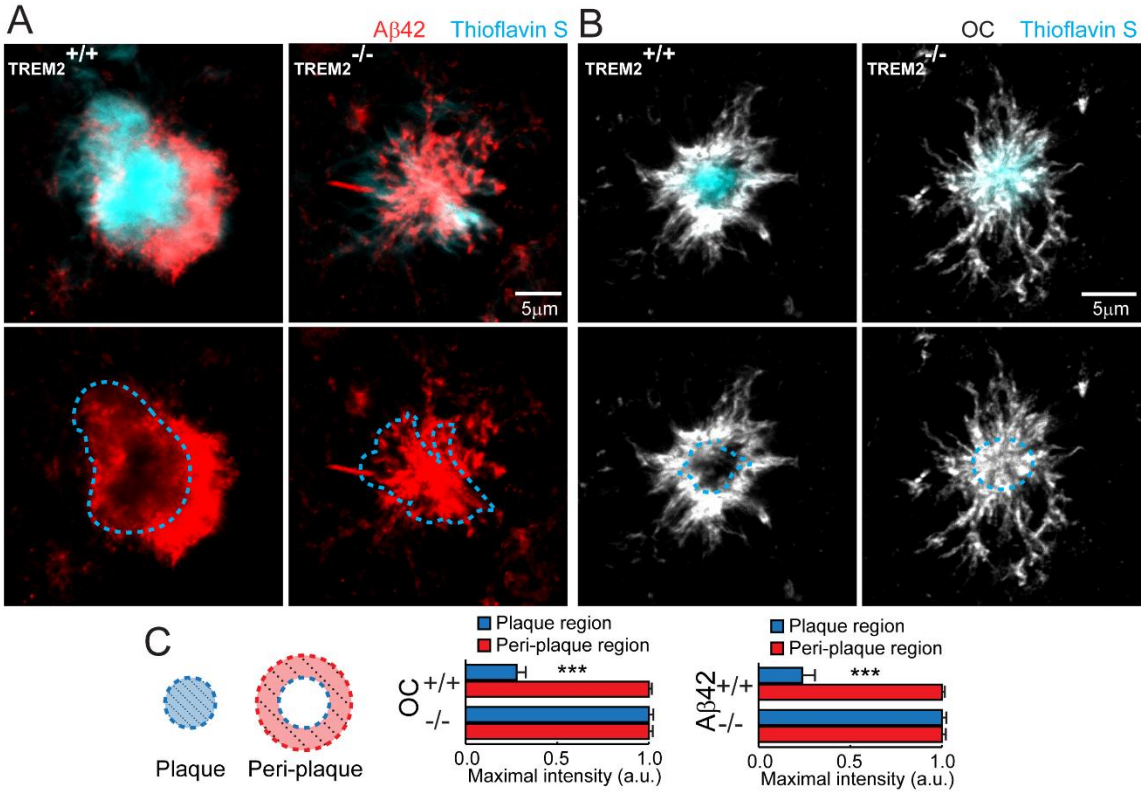

TREM2 deficiency reduces plaque compactness as revealed by increased penetration of Aβ antibodies to the plaque core

(**A** and **B**) Confocal images of anti-Aβ42 (red) and anti-oligomeric amyloid (OC; white) immunohistochemistry of thioflavin S positive plaques (cyan) in 5XFAD brain tissue with different Trem2 genotypes. Lower panels show fluorescence channel with antibody staining only. Cyan dashed lines indicate thresholded plaque perimeter (core). (**C**) Quantification of anti-Aβ42 and anti-OC antibody staining within plaque core and peri-plaque regions in Trem2+/+ and Trem2-/- mice. N=10 plaques in each group. Student t-tests were used for statistical comparison. ***: $p<0.001$; a.u.: arbitrary unit. All analyses were performed with neocortical plaques.

Figure S6 (related to Figure 6)

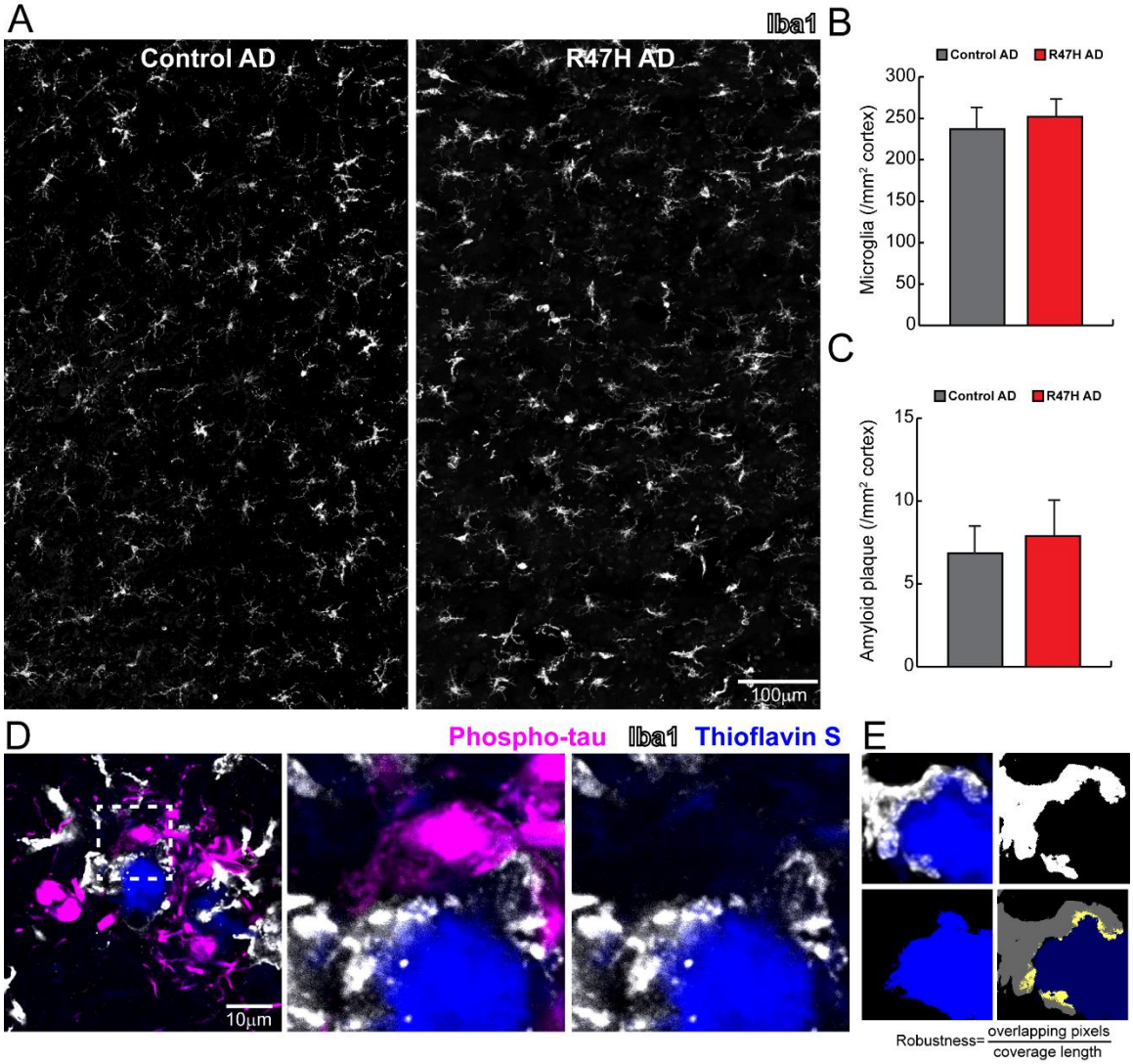

R47H TREM2 mutation disrupts microglia envelopment of amyloid plaques but has no effect on resting state microglia nor overall plaque burden

(**A**) Confocal images of microglia, labeled by anti-Iba1 immunostaining (white), in plaque-free cortical regions from postmortem human brains with and without R47H mutation. (**B**) Quantification of the number of microglia in cortical regions of human brains with and without R47H mutation. (**C**) Quantification of the number of plaques (all subtypes) in gray and white matter of human brains with and without R47H mutation. N=5 human subject for all quantifications. No statistical significance was detected using Student T-test. (**D**) Images of the stereotypical interaction between microglia and amyloid plaques. Microglia (anti-Iba1 labeling, white) spread their processes closely onto plaque (blue) surfaces, while they do not display any obvious interaction with adjacent dystrophic neurites (anti-phospho-tau labeling, magenta). Middle and right panels show zoomed split channel images from dashed box in the left panel. (**E**) Example of image processing to measure the "closeness" of the interaction between microglia processes and the amyloid plaque surface as "Barrier Robustness", see quantification in **Figure 6H**. Robustness was calculated as the number of overlapping pixels between microglia process and amyloid plaques (yellow pixels in the right bottom panel) normalized by the length of the plaque perimeter covered by the microglia process.

Figure S7 (related to Figure 6 and 7)

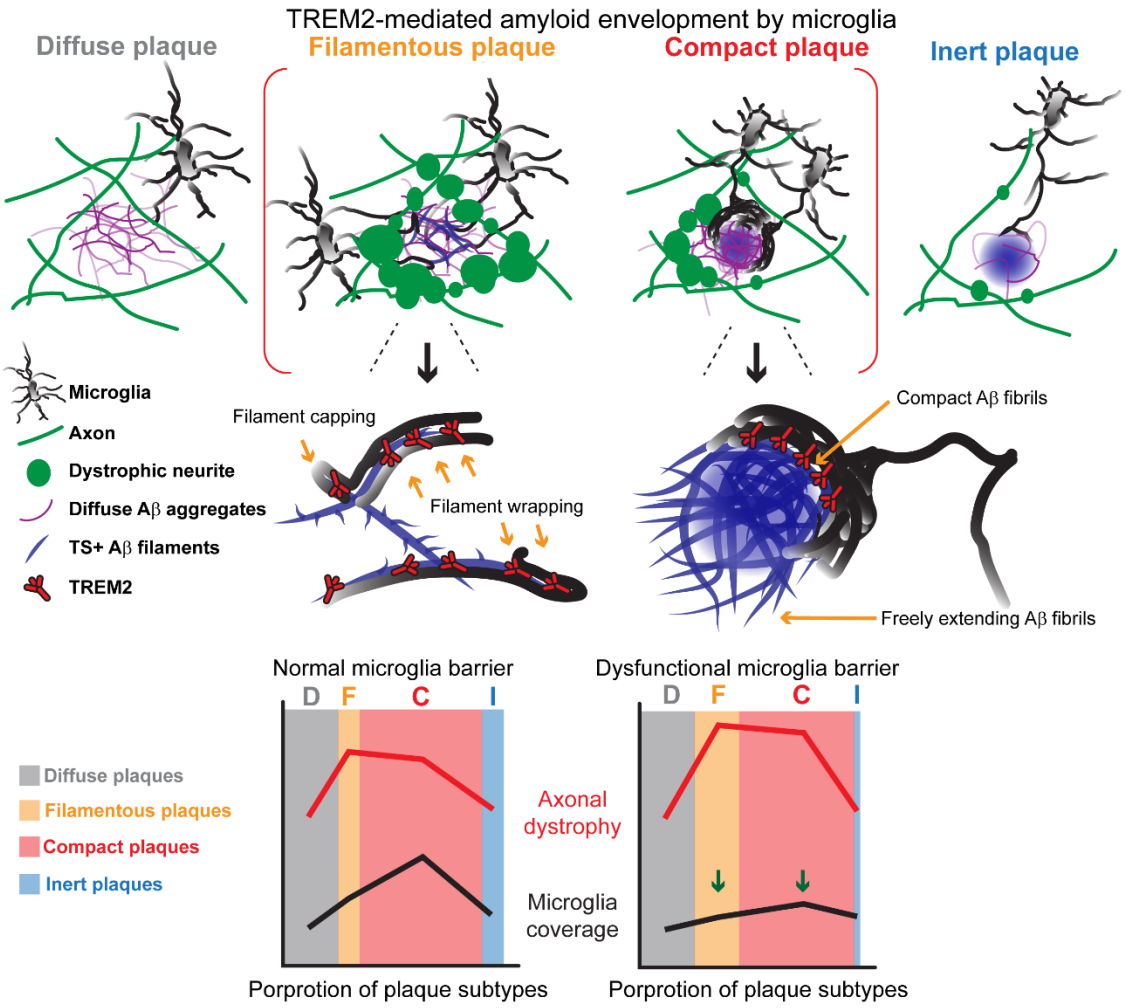

Summary diagram of microglia barrier function and molecular control by TREM2

1) Unlike diffuse amyloid plaques (thioflavin S negative), early filamentous amyloid deposits (thioflavin S positive) extensively attract polarized microglia processes that intermingle with it.

2) Diffuse plaques do not have dystrophic neurites around them while filamentous plaques have a surprisingly large degree of neuritc dystrophy suggesting that adoption of a beta-sheet rich conformation triggers axonal toxicity.

3) TREM2-rich microglia processes closely envelope individual thioflavin S positive amyloid filaments and small fibril clusters. Compact amyloid plaques are also robustly covered my microglia processes.

4) This interaction leads to thicker and shorter amyloid fibril bundles with reduced branching and to more compact amyloid deposits.

5) TREM2 haplodeficiency in humans and in mice causes a severe abnormality in the ability of microglia to polarize towards amyloid deposits. This leads to a more branched and less compact plaque phenotype with an overall increase in fibril surface area contacting adjacent neuronal processes. In both filamentous and compact plaques, the decreased compaction and increased fibril surface area caused by TREM2 haplodeficiency was associated with marked increases in the degree of axonal dystrophy and neuritic tau

hyper-phosphorylation. This strongly suggests that microglia envelopment of amyloid deposits plays a critical neuroprotective role by compacting toxic fibrils and insulating from the adjacent neuropil (Microglia “barrier function”).

6) In humans, we observed a subpopulation of plaques that had extremely high thioflavin S labeling and lacked enveloping microglia processes. Interestingly, these plaques demonstrated very little neuritic dystrophy. This suggests two possible explanations: one in which these are terminal plaques in which axonal dystrophy has peaked and subsequently disappeared due to degeneration. A second and more intriguing hypothesis is that these plaques were highly compacted at early stages such that very little dystrophy developed around them, and microglia no longer get attracted to them due to their exceptional degree of compaction.

7) Loss of the protective microglia barrier function in TREM2 deficiency does not change the total number of amyloid deposits, but instead leads to an increased proportion of filamentous plaques. Dysfunctional microglia barrier in TREM2 haplodeficiency and potentially due to microglia senescence in sporadic AD leads to more severe axonal dystrophy around amyloid deposits.

Table S1 (related to Figure 1)

	Vendor	Clone	Host	Species	Cat#	IHC result
Trem2	Santa Cruz	B-3	mouse	human	sc-373828	-
	Santa Cruz	G-16	goat	human	sc-22634	-
	R&D Systems		sheep	mouse	AF1729	+++
	Abcam		goat	human	ab85851	-
DAP12	Santa Cruz	A-20	goat	human; mouse	sc-7855	-
	Santa Cruz	C-20	goat	human; mouse	sc-7853	-
	Santa Cruz	FL-113	rabbit	human; mouse	sc-20783	-
	LS Bio		goat	human; mouse	B3718	-
	LS Bio		rabbit	mouse; human	B9453	++

Trem2 and DAP12 antibodies tested in this study

Heat-induced sodium citrate antigen retrieval was performed for all the antibodies tested with the following protocol: tissue was boiled in 50mM sodium citrate solution with 0.05% tween-20 at 95 degrees for 45 minutes and then washed with PBS 3 times before staining.

Table S2 (related to Figure 6 and 7)

Case ID	TREM2 R47H	Gender	Age	Braak Stage	Brain bank	Comorbid pathology
0013	Mutant	Male	87	V	BSHRI	Lewy body disease
0414	Mutant	Female	76	VI	UW-ADRC	
1462	Mutant	Female	89	V	UW-ADRC	Lewy body disease
5168	Mutant	Female	87	VI	UW-ADRC	Parkinson's disease; Meningitis
5219	Mutant	Male	86	VI	UW-ADRC	
0195	Control	Male	83	V	UW-ADRC	
0550	Control	Female	89	V	UW-ADRC	
1353	Control	Female	92	VI	BSHRI	Cerebral white matter rarefaction
1375	Control	Male	77	VI	BSHRI	Moderate Purkinje cell loss
1406	Control	Male	85	V	BSHRI	Microscopic infarct in left hippocampus
M6	Mutant	Female	87	V	MAYO	
M17	Mutant	Male	88	IV	MAYO	
M20	Mutant	Female	74	V	MAYO	
M21	Mutant	Male	76	VI	MAYO	
M22	Mutant	Female	77	VI	MAYO	Lewy body disease
M6c	Control	Female	84	IV	MAYO	
M20c	Control	Female	77	VI	MAYO	
M21c	Control	Male	74	V	MAYO	
M22c	Control	Female	83	V	MAYO	Lewy body disease

Donor information of the postmortem human AD brain tissues used in this study

All cases were confirmed with amyloid pathology in the brain tissue. All cases used in this study were Caucasians with the ApoE3/E4 genotype. Brain slices from the middle frontal gyrus (cortex) were used for all analyses in this study. BSHRI; Banner Sun Health Research Insitute (Sun City, AZ). UW-ADRC; University of Washington, Alzheimer's Disease Research Center (Seattle, WA). MAYO; Mayo Clinic (Jacksonville, FL).

Supplemental Experimental Procedures

Reagents

Anti-Iba1 polyclonal antibody (Wako, 019-19741, RRID:AB_839504), anti-Coronin1a (Santa Cruz, clone 14.1, sc-100925, RRID:AB_2291951) and anti-CD11b (AbD Serotec, clone 5C6, MCA711G, RRID:AB_323167) were used to label microglia. Anti-mouse TREM2 antibody (R&D systems, AF1729, RRID:AB_354956) was used to detect TREM2 protein. Anti-DAP12 antibody (LifeSpan Biosciences, LS-B9453, originally RRID:AB_10828136) was used for staining DAP12. Anti-Ki67 antibody (Abcam, ab16667, RRID:AB_302459) was used to label dividing cells. Anti-GFAP antibody (DAKO, Z0334, RRID:AB_10013382) was used to label astrocyte. Anti-NeuN antibody (EMD Millipore, ABN78, RRID:AB_11211087) was used to label neuronal nucleus. Anti-phospho-tyrosine antibody (EMD Millipore, clone 4G10, 05-321, RRID:AB_309678) was used to detect phosphorylated tyrosine. Anti-Lamp1 antibody (DSHB, 1D4B, RRID:AB_2134500) was used to label neuritic dystrophy in mice and anti-APP antibody (ThermoFisher Scientific, LN27 13-0200, RRID:AB_86542) and anti-Phospho-PHF-tau pSer202+Thr205 (ThermoFisher Scientific, AT8 MN1020, RRID:AB_223647) were used for human. Anti-Aβ 17-24, 4G8 antibody (BioLegend, 800701, RRID:AB_2564633) was used to label amyloid plaques. Anti-CD68 antibody (AbD serotec, MCA1957, RRID:AB_322219) was used to label microglial phagosomes. Alexa dye conjugated secondary antibodies were used (ThermoFisher Scientific). For STORM microscopy (see below), anti-Aβ antibody (Cell Signaling Technology, #2454, RRID:AB_2056585) and goat anti-rabbit-Alexa 647 secondary antibody (ThermoFisher Scientific, A-20991, RRID:AB_2535705) were used to label amyloid fibrils. Thioflavin S (Sigma-Aldrich, T1892, 2% w/v stock solution, 1:10k staining) was used for labeling amyloid deposits in fixed slices. DAPI (Sigma-Aldrich, D9542) was used for labeling cell nuclei.

Confocal analyses

Measurements of plaque sizes were collected using z-axis projections of 5 optical slices aligned along the center of the plaques. Plaque regions were distinguished using a threshold fluorescence intensity that was two standard deviations above the average fluorescence intensity of the image as previously reported. Classification of thioflavin S positive or negative plaques were done by scrolling through the z-stack and

judging manually. Only plaques that were completely within the whole depth of the z-stack were counted in this analysis.

Microglia barrier around filamentous plaques was defined as 1) processes closely tracking along and wrapping around individual amyloid fibril and 2) processes forming cap-like structures at the end of amyloid filament. These events were manually quantified from the whole z-stack of individual plaque. Microglia barrier around compact plaques was defined as activated microglia processes tightly wrapping around amyloid plaques, with Iba1 expression higher than the baseline microglial processes. In order to measure the compact plaque coverage by microglia barrier, a 3-slice z-projection at the center of the segmented plaque was made. The Iba1 channel was then thresholded using the Iba1 fluorescence intensity in the cell body as the cutoff value. The contact points of plaque perimeters with microglia processes was then determined manually. And the proportion of the plaque perimeter covered by microglia barrier was determined by measuring the distances between contact points along plaque perimeter. For measuring barrier robustness, theresholded images were generated for both the Iba1 and thioflavinS channel. The number of pixels overlapping between the two channels were counted and then divided by the plaque perimeter covered by microglia barrier.

For measuring dystrophic neurites, a 3-slice z-projection through the center of the plaque core was made for each segmented plaque. The dystrophy area was determined by threshold the image with 150% fluorescent intensity of a background region in the same channel. To estimate the volume of dystrophy, the measured area was converted to volume assuming a spherical geometry. Plaque volume was subtracted from the dystrophy volume.

For measuring the degree of dystrophic neurites corresponding to microglia covered and not covered plaque microregions, the total area of dystrophic neurites was radially divided into pie-shaped regions based on microglia coverage. A pie-shaped selection was made by connecting the center of the plaque and the points used for measuring microglia barrier, and extending outward until crossing the dystrophic neurites border. Subsequently, the area of dystrophic neurites was measured within each pie-shaped selection and assigned to microglia covered and not covered regions. The assigned area of dystrophic neurites was further normalized by the degree of microglia coverage:

$$Dystrophic\ neurite\ (covered/\ not\ covered) = \frac{\frac{Dystrophy\ area\ in\ covered\ regions}{Microglia\ coverage}}{\frac{Dystrophy\ area\ in\ not\ covered\ regions}{(360 - Microglia\ coverage)}}$$

If the above ratio is less than 1, it indicates the microglia coverage is relatively protective in preventing dystrophic neurites around plaques. Geometric mean of all the plaques measured in each subject was used as the average measurement for each person.

For measuring Trem2 immunostaining, fluorescence intensities were measured from a 5μm z-projection through the center of desired structure. The region of interest was determined by manual tracing. To measure phosphor-tyrosine fluorescence intensities, a selection of 4μm width was created along the perimeter of the plaque, using the "XOR" function between "Enlarge" +2 and -2 regions.

For measuring thioflavin S fluorescent intensity and circularity, a z-projection of maximal fluorescence intensities across 5 optical slices through the center of the plaque core was made. The plaque area was selected by "isodata" threshold and thioflavin S fluorescent intensity was measured from the selection. The selection was also used to calculate circularity by the following equation: circularity = 4π x area / $(\text{perimeter})^2$.

For measuring microglia polarization, microglia cells were segmented from the tiled images described above. A z-projection at the center of the cell body was made across 5 optical sections. The somata of microglia was traced manually and the cell's territory was selected using "Enlarge" function in FIJI at 20μm. The donut shape selection was divided radially into 8 pies, each representing roughly 45 degree space surrounding the cell. Fluorescence intensity of Iba1 staining was measured in each of the 8 pie areas and polarization index was calculated as the coefficient of variation for the 8 regions (ratio of the standard deviation to the mean). In addition to fluorescence intensity, thresholded area of the Iba1 staining was also analyzed in the same method and the results were consistent with using fluorescence intensity (not shown).

For measuring Aβ phagocytosis by microglia, a z-projection was made for each microglia to cover the total volume of the somata. The CD68 fluorescent channel was thresholded using "IsoData" preset in FIJI and total area was measured using "Analyze Particle" function. The 4G8 fluorescent channel was also

thresholded using “IsoData” and the intra-microglia amyloid was measured by multiplying the 4G8 puncta area and the fluorescence intensity.

STORM analyses

Reconstructed images were imported into FIJI via “BioFormat” plugin for analyses. Images were converted to 16-bit before measurements. To measure different fibril organization areas in each plaque, the image was first thresholded with “isodata” to measure the total area of the plaque. Subsequently, the compact core areas were manually traced based on the marked differences in fluorescence intensity. Next, the mesh-like structures were traced based on the definition where fibril directions cannot be determined confidently. Diffuse fibril areas were then calculated by subtracting these two compact areas from the total area of the plaque.

To measure the width of individual Aβ fibril, a 10-pixel wide line selection was made horizontally from the fibril. Fluorescence intensity profiles from the line was recorded and plotted against distance. The plotted line was then fitted with a Gaussian curve and width was determined by 2.35 times of the standard deviation of the fitted curve.

To measure the frequency of the branched structures, single segments of fibrils without intersecting with other fibrils were chosen. Branched structure was defined as fibrils orthogonally extending from the main Aβ fibril stem. The tip of the branches needs to exceed 8 pixels (~40nm) away from the main fibril in order for this structure to be counted.

Estimation of plaque surface area change in Trem2 deficient mice

The following equations are used to estimate the surface area:

Surface area = Surface area of individual fibril * Number of diffuse fibrils.

Surface area of individual fibril = (π * (fibril diameter) * (fibril length)) + surface area of individual branched structure * Densities of branched structures * fibril length

From our STORM imaging results, average fibril diameter in Trem2 +/+ is 67nm, Trem2 +/- is 56nm and Trem2 -/- is 46nm, length +/+ 231nm, +/- 396nm, -/- 442nm.

Next in order to estimate the area of individual branched structures, we assume the average dimensions of these structures are 20nm in diameter and 80nm in length. Therefore surface area of individual branch structure = $\pi * 20 * 80$ $(nm)^2$. The densities of branched structures in Trem2 +/+ is 0.5, Trem2 +/- is 2.1 and Trem2 -/- is 3.2, per 500nm length of fibril.

Therefore the surface area of individual fibrils can be calculated:

Trem2 +/+: $(\pi * 67 * 231) + (\pi * 20 * 80 * 0.5 / 500 * 231) = 49{,}756$ $(nm)^2$

Trem2 +/-: $(\pi * 56 * 396) + (\pi * 20 * 80 * 2.1 / 500 * 391) = 77{,}988$ $(nm)^2$

Trem2 -/-: $(\pi * 46 * 442) + (\pi * 20 * 80 * 3.2 / 500 * 442) = 78{,}054$ $(nm)^2$

This can be normalized to Trem2 +/+ 100%, Trem2 +/- 157% and Trem2 -/- 157%.

Next, Number of diffuse fibrils is estimated assuming equal amount of amyloid material for each plaque. Our results indicate that 30% of the total material in Trem2 +/+ are diffuse fibrils, 60% in Trem2 +/- and 85% in Trem2 -/-. This translates to 2 times in the number of fibrils in Trem2 +/- and 2.83 times in Trem2 -/- compared to Trem2 +/+.

Taken together, we estimate Trem2 +/- increased surface area of individual plaque to 157% * 2 = 314% and Trem2 -/- to 157% * 2.83 = 444% compared to Trem2 +/+.